LSD-induced increase of Ising temperature and algorithmic complexity of brain dynamics

Giulio Ruffini[1,2,3*], Giada Damiani[1], Diego Lozano-Soldevilla[1], Nikolas Deco[1] , Fernando E. Rosas[4,5,6,7], Narsis A. Kiani[8,9], Adrián Ponce-Alvarez[10], Morten L. Kringelbach[11,12,13], Robin Carhart-Harris[4], Gustavo Deco[14,15,16,17]

1 Neuroelectrics Barcelona, Av. Tibidabo 47b, 08035 Barcelona, Spain
2 Starlab Barcelona, Av. Tibidabo 47b, 08035 Barcelona, Spain
3 Haskins Laboratories, 300 George Street, New Haven, CT, 06511, USA
4 Centre For Psychedelic Research (Department of Medicine), Imperial College London, London, UK
5 Data Science Institute, Imperial College London, London, UK
6 Centre for Complexity Science, Imperial College London, London, UK
7 Department of Informatics, University of Sussex, Brighton, UK
8 Algorithmic Dynamics Lab, Center of Molecular Medicine, Karolinksa Institutet, Stockholm, Sweden
9 Oncology and pathology Department, Karolinksa Institutet, Stockholm, Sweden
10 Center for Brain and Cognition, Computational Neuroscience Group, Department of Information and Communication Technologies, Universitat Pompeu Fabra, Roc Boronat 138, Barcelona, 08018, Spain
11 Centre for Eudaimonia and Human Flourishing, University of Oxford, Oxford, UK
12 Department of Psychiatry, University of Oxford, Oxford, UK
13 Center for Music in the Brain, Department of Clinical Medicine, Aarhus University, Aarhus, Denmark
14 Institucio Catalana de Recerca i Estudis Avançats (ICREA), Universitat Pompeu Fabra, Computational Neuroscience, Barcelona, Spain
15 Institució Catalana de la Recerca i Estudis Avançats (ICREA), Passeig Lluís Companys 23, Barcelona, 08010, Spain
16 Department of Neuropsychology, Max Planck Institute for Human Cognitive and Brain Sciences, 04103 Leipzig, Germany
17 School of Psychological Sciences, Monash University, Melbourne, Clayton, VIC 3800, Australia

* giulio.ruffini@neuroelectrics.com

Abstract

A topic of growing interest in computational neuroscience is the discovery of fundamental principles underlying global dynamics and the self-organization of the brain. Statistical physics offers powerful tools to analyze complex many-body systems and has delivered computational models such as the generalized Ising model, one of the simplest systems displaying phase transitions. Prior work has shown that different brain states may be mapped into pairwise maximum entropy Ising models at various levels of criticality. Here, we use this framework to analyze resting state fMRI BOLD data collected in an earlier study from fifteen subjects in a control condition (placebo) and during psychedelic ingestion (LSD). To address the limited quantity of data available from typical BOLD studies, we create an "archetype" Ising model representative of the entire dataset using the AAL parcellation. The archetype is then personalized for each individual and condition by adjusting the system temperature. We analyze the resulting temperatures to show that the models are near criticality but in the paramagnetic (disordered) phase. Second, the individualized Ising temperatures increase significantly under the effects of LSD compared with the placebo condition ($p = 9 \times 10^{-5}$). Next, we estimate the Lempel-Ziv-Welch (LZW) complexity of the binarized BOLD data and the synthetic data generated with the individualized model using the Metropolis algorithm for each participant and condition. The LZW complexity computed from experimental

data reveals a weak statistical relationship with condition ($p = 0.04$ one-tailed Wilcoxon test) and none with Ising temperature ($r(13) = 0.13, p = 0.65$), presumably because of the limited data. However, the LZW complexity computed using synthetic data from the personalized archetype model correlates strongly with individualized temperature ($p = 2.7 \times 10^{-6}$) and hence with condition ($p = 9 \times 10^{-5}$, one-tailed Wilcoxon test). Then we explore algorithmic complexity using the block decomposition method (BDM). The BDM complexity of the experimental data displayed a robust correlation with Ising temperature ($r(13) = 0.56, p = 0.03$) and a weak but significant correlation with condition ($p = 0.04$, one-tailed Wilcoxon test). We also calculated the BDM complexity of the synthetic data generated by the model, which correlated strongly with Ising temperature ($r(13) = 0.97, p = 8.9 \times 10^{-10}$) and hence condition ($p = 2 \times 10^{-4}$, one-tailed Wilcoxon test). This study suggests, together with prior ones, that the effects of LSD increase the complexity of brain dynamics. In agreement with earlier work using the Ising formalism, we find the brain state in the placebo condition is already above the critical point, with LSD resulting in a shift away from criticality into a more disordered state.

Author summary

We study criticality features of brain dynamics under LSD in a within-subject study using the Ising model formalism and algorithmic complexity using Lempel-Ziv and the Block Decomposition methods. Personalized Ising models are created by first using fMRI BOLD data from all the subjects and conditions to create a single Ising "archetype" model — which we can interpret as the average model of the data at unit temperature — and then by adjusting the model temperature for each subject and condition. We find that the effects of LSD translate into increased BOLD signal complexity and Ising temperature, in agreement with earlier findings and predictions from existing theories of the effects of psychedelics, such as the relaxed beliefs under psychedelics (REBUS), the anarchic brain hypothesis [4], and the algorithmic information theory of consciousness (KT) [64, 67]. However, in contrast with some of the previously cited theories, we find that the system in the placebo condition is already in the paramagnetic phase—above the critical point—with ingestion of LSD resulting in a shift away from Ising criticality into a more disordered state.

Introduction

The complex features displayed by the emergent neural dynamics of the human brain are in many ways reminiscent of behaviors of paradigmatic systems in statistical physics [10, 9, 16, 13, 24, 23, 25, 53, 80]. For example, just as condensed materials can transit between ordered (e.g., solid and liquid) or disordered (e.g., gas) phases, neural networks can undergo phase transitions going between highly regular and highly unsynchronized activity. Of particular interest are dynamics of systems poised close to phase transitions, where co-called critical points display a balance of order and disorder that has been conjectured to be crucial for living organisms [46]. At critical points, non-trivial collective patterns spanning all scales are observed, giving rise to a rich repertoire of short- and long-range correlations. The fluctuations in critical systems are highly structured, obeying fundamental physical principles rooted in the system's symmetries — which are shared by many systems despite their underlying constituency, establishing 'universality classes' of large-scale coordinated activity [29].

Theoretical work indicates that computation and information dynamics in complex systems display special features at critical points [72, 47, 50, 51, 22]). Building on these

insights, criticality has been suggested as a useful principle to account for the brain's inherent complexity that is required to guide behavior in rich environments by processing various sources of information [18, 20, 12, 74, 9, 32, 33]. Furthermore, it has been found that systems in nature often tune themselves into a critical state — a principle known as 'self-organized criticality' [40, 61, 11]. It has been proposed that neural systems may self-organize, evolutionary and developmentally, through homeostatic plasticity rules that result in the system arriving near critical states [58, 34, 5].

Building on this pioneering work, this paper aims to leverage tools from the statistical physics literature to study brain dynamics that support different states of consciousness. Here we focus in the altered state of consciousness induced by LSD, a psychedelic substance that is recently harnessing attention for its therapeutic potential for addressing mental disorders such as anxiety, depression, or substance addiction [8, 27, 30, 41, 44]. While our understanding of how LSD work at the neuronal and pharmacological levels is relatively well developed [48, 56, 5], there is a need to deepen our understanding of its effects at the whole-brain level to better explain and predict the outcomes of psychedelic interventions—such as psychedelic-assisted therapy [8, 52, 60]. It has been argued that the observed expansion of the repertoire of functional patterns elicited by hallucinogenic substances can be understood as being driven by an enhancement of brain entropy [5]. In turn, this may take place while the brain is moving closer to criticality, with this being related to the relaxation of high-level cognitive priors [4, 67], which in turn may lead to a favorable context for conducting psychotherapy [28, 4]. Studies on functional neuroimaging regarding LSD effects have shown initial evidence of the mechanistic alterations on brain dynamics at the network level, with the majority of the findings suggesting a relative weakening of usual functional configurations giving place to an increase of brain entropy, global functional integration, and more flexible brain dynamics [6, 7, 8, 73, 59, 75, 5, 49].

Given the theoretical and empirical evidence suggesting that LSD induces a shift towards a broader repertoire of neural patterns enabled by more flexible dynamics, the present study aims to characterize the underlying neural mechanisms responsible of these effects via mathematical and computational modeling tools from statistical physics and phase transitions. Specifically, we leverage maximum entropy models — the most parsimonious models one can build following statistical physics principles [38, 39] — to describe the coordinated activity of various brain areas as captured by BOLD signals. By building individualized computational models for LSD and placebo conditions, we aim to observe differences with respect to the model's temperature: a parameter that describes the system's randomness. In particular, a low temperature amplifies distinctions between energy levels and hence a higher dissimilarity between the likelihood of occupancy of different states; conversely, a high temperature 'flattens' the energy landscape, which allows more states to become accessible. Additionally, the system's temperature regulates its phase transitions, and hence its value establishes how far it is from criticality. In addition, given the potential relationship between signal diversity, algorithmic complexity, criticality, and brain state, we explore complexity metrics characterizing the two conditions in the data with the hypothesis that complexity correlates with system temperature [64, 63, 67].

Materials and methods

Experimental protocol and fMRI BOLD data

We use a dataset that consists of two time series under LSD effects and two for the placebo condition for each of 15 participants. Details of the data acquisition process can

be found in detail in [8, 17], and we only provide a summary here. The study was approved by the National Research Ethics Service committee London-West London and was conducted in accordance with the revised declaration of Helsinki (2000), the International Committee on Harmonization Good Clinical Practice guidelines, and National Health Service Research Governance Framework. Imperial College London sponsored the research, which was conducted under a Home Office license for research with schedule 1 drugs. Written informed consent was given and data was de-personalized (anonymized) prior to analysis. A group of 15 participants (4 women; mean age, 30.5±8.0) were recruited by personal spoken communication and provided with written consent to participate in the experiment after a briefing and screening study for physical and mental health. It included and electrocardiogram (ECG), urine and blood tests, plus a psychiatric test and drug historical. Participants under 21 years, with psychiatric diseases, family history of psychotic disorders, experience with psychedelics, pregnancy, problems with alcohol (>40 units per week), or any other medically significant condition that could affect the study were excluded. Participants attended twice the laboratory (once per condition), with a separation of 2 weeks. The order of these was alternated across participants without giving the information of the experimental condition used in each session. With the help of a medical doctor, after the tests, a cannula was inserted into a vein in the antecubital fossa. The dose consisted of 75 mg of LSD via a 10ml solution proportioned over two minutes with an infusion of saline afterward. After this, participants were suggested to lie relaxed with closed eyes inside the MRI scanner. Participants provided subjective reports of the drug effects after a 5 to 15 minutes period from the administration of the drug. The peak effects were reported to be after 60–90 minutes of the dose. Subsequently, effects were generally constant for four hours. The scanning was done approximately after 70 minutes for the dose and lasted a full hour. BOLD scanning was composed of three resting state scans of seven minutes. The middle one incorporated listening to two excerpts of music from two songs by ambient artist Robert Rich. For our analysis here, we exclude the scan with music. Thus, the dataset includes four scans (two under LSD, two in the placebo condition) for each of the fifteen subjects (for a total of sixty).

Parcellated data series

Preprocessing of the fMRI BOLD data using FSL tools (FMRIB's Software Library, `www.fmrib.ox.ac.uk/fsl`) for the generation of parcellated (region-averaged) BOLD time series is described in detail in [17]. Only the 90 AAL atlas cortical and subcortical non-cerebellar brain regions were considered [77] (see Table 3 in Appendix A).

Data binarization

To build an Ising model from the data, we transform the fMRI BOLD data series for each parcel into a binary format. This is done by using a threshold. Each data point is assigned a value of +1 if its value is greater than the threshold, and -1 otherwise, with the threshold set to the median of the data in the parcel. Hence the median of the thresholded time series of each voxel is zero and its entropy is maximal.

Data analysis of fMRI series

Lempel-Ziv complexity

Lempel-Ziv (LZ) refers to a class of adaptive dictionary compression algorithms that parse a string into words and use increasingly long reappearing words to construct a dictionary. Compression is achieved by pointing to the identifiers of words in the

dictionary [45, 79, 14]. LZ algorithms are universally optimal—their asymptotic compression rate approaches the entropy rate of the source for any stationary ergodic source [14], $l_{LZ} \to n\mathcal{H}$.

After applying the algorithm to a string of length n, we obtain a set of words in a dictionary of length $c(n)$ that can be thought of as a first complexity metric [82]. The description length of the sequence encoded by LZ can be approximated by the number of words seen times the number of bits needed to identify a word, and, in general, $l_{LZ} \approx c(n) \log_2 c(n) \lesssim n$. We note that LZ provides an upper bound on algorithmic complexity, but, given its reduced programming repertoire (LZ is the Kolmogorov complexity computed with a limited set of programs that only allow copy and insertion in strings [42]), LZ fails, in general, to effectively compress random-looking data generated by simple, but highly recursive programs, e.g., an image of the Mandelbrot set (deep programs [68, 67]). As a further example of these limitations, consider a string concatenated with its bit-flipped, "time-reversed", or dilated version. Such simple algorithmic manipulations will not be detected and exploited by LZ. Despite this, LZ can be useful to study the complexity of data in an entropic sense. To use LZW, we need first to transform numeric data into a list of symbols. Here we binarize the data to reduce the length of strings needed for the algorithm to stabilize. A reasonable strategy in the study of algorithmic information content of EEG data is to preserve as much information as possible in the resulting transformed string. In this sense, using methods that maximize the entropy of the resulting series is recommended. Here, as discussed above, we use the median of the data as the threshold.

Two associated metrics derived from LZ compression are commonly used: $c(n)$ and l_{LZ}. Of the two, the latter is more closely related to Kolmogorov complexity or description length. A natural way to normalize this metric is to divide description length by the original string length n, $\rho_0 = l_{LZ}/n \to \mathcal{H}$, with units of bits per character. Here, we analyze the lattice data by computing ρ_0 for each sample of a set of lattice realizations (with synthetic data) or by concatenating them for a global measure (with real data). The former allows for a plot of the standard deviation of the measure with synthetic data using the Metropolis algorithm as a function of temperature (Figure 3), but does not change the behavior with an inflection point near the model's critical temperature. To calculate a global measure of LZ complexity using the experimental data, we first concatenated the data from all subjects, conditions, and sessions, then flattened it along the spatial dimension first and then time. Secondly, we compressed the flat binarized data with the LZ algorithm and saved the output "archetype dictionary", which was used as the initial dictionary to compress the data from all the subjects in the two conditions, LSD and placebo (comparison by condition), and also per subject (comparison by condition and subject). The "archetype dictionary" was built by concatenating first the LSD data for all subjects and sessions and then the placebo data because we were forced to make a choice when flattening the array. However, we checked whether concatenating the placebo data before the LSD changed the results, and the difference was negligible. For details and code used to compute LZ complexity—we use the Lempel-Ziv-Welch (LZW) variant—see [79, 66].

Block decomposition method

The Block Decomposition Method (BDM) [81] combines the action of two universally used complexity measures at different scales by dividing data into smaller pieces for which the halting problem involved can be partially circumvented, in exchange for a huge calculation based upon the concept of algorithmic probability and extending the power of the so-called Coding Theorem Method (CTM). The calculation, however, has been precomputed and hence can be reused in future applications by exchanging time for memory in the population of a precomputed look-up table for small pieces. BDM is

used to account for both statistical regularities and algorithmic ones, and is sensitive enough to capture small changes in the complexity and invariant to different descriptions of the same object. It, therefore, complements the use of lossless compression algorithms to calculate upper bounds of algorithmic complexity.

Ising model

Abstract frameworks from statistical physics can shed light on understanding emerging phenomena in large networks such as phase transitions in systems where nodes — neurons or cortical columns here — interchange information under the assumptions of the maximum entropy principle [38, 39, 71]. The description of systems with many degrees of freedom can be summarized by coarse-graining variables (describing macrostates), a step that introduces statistics into modeling. At the so-called critical points, observable quantities such as diverging correlation length or susceptibility to external perturbations reveal singularities in the limit as the number of degrees of freedom goes to infinity. At these transitions, from order to disorder, there is a loss of sense of scale, with fractal properties in energy and information flow.

In this context, elements such as neurons, columns, or brain regions are modeled by spins (i.e., with two states, up or down, on or off) with pair interactions and the emerging statistical properties of large networks of these elements are studied under different conditions (temperature or excitability, or an external magnetic or electric field). The prototypical simplest system in this context is the classical 2D Ising model, which features nearest neighbor interactions and a phase transition. This model has been shown to be universal, i.e., that all the physics of every classical spin model (with more general types of interactions) can be reproduced in the low-energy sector of certain "universal" models such as the 2D Ising model [15]. This fact reflects the intrinsic computational power of near-neighbor interactions. In fact, Ising models have been shown to be universally complete [31, 43], with a map between any given logic circuit to the ground states of some 2D Ising model Hamiltonian. On the other hand, the fact the brain exhibits characteristics of criticality that may be modeled by systems such as the Ising model is now well established, with ideas that go back to pioneers such as Turing, Bak [10], and Hopfield [36]. There is further evidence that the dynamics of the healthy brain occupy a sub-critical zone (see [5] and references therein).

The 2D Ising model used here is slightly more general than the original one, as it allows for arbitrary pair interactions (not just near neighbors, see next section). It is given by the energy or Hamiltonian of the lattice of N spins,

$$\mathcal{H}[\sigma] = -\sum_{i<j\leq N} J_{ij}\sigma_i\sigma_j - \sum_i h_i\,\sigma_i \tag{1}$$

where σ_i denotes the orientation of each spin in the lattice (± 1), J_{ij} is the coupling matrix (with pairs counted once) and $\boldsymbol{h}$ is an external magnetic field applied independently at each site.

Maximum entropy principle derivation of Ising model

The Ising model, which was originally proposed to describe the physics of ferromagnetic materials, can be seen to arise naturally from the Maximum Entropy Principle (MEP) [38]. The MEP is used to find an appropriate probability distribution given some constraints, e.g., derived from data. It states that the probability of finding a given spin configuration σ can be inferred from a simplicity criterion: given some data-derived constraints — which here will be that the mean spin and spin correlation values of the model should match that of the data — the probability function we should use is the

one that fits the constraints but has otherwise maximal Shannon entropy. It turns out that the probability distribution function of observing a given spin configuration $\boldsymbol{\sigma}$ (bold symbols indicate an array) in thermal equilibrium (at unit temperature without loss of generality) is given by the Boltzmann distribution [24]

$$P(\boldsymbol{\sigma}|\boldsymbol{h},\boldsymbol{J}) = \frac{e^{-\mathcal{H}(\boldsymbol{\sigma}|\boldsymbol{h},\boldsymbol{J})}}{\sum_{\{\boldsymbol{\sigma}'\}} e^{-\mathcal{H}(\boldsymbol{\sigma}'|\boldsymbol{h},\boldsymbol{J})}} \tag{2}$$

with $\mathcal{H}$ given in Equation 1.

Estimation of archetype parameters using maximum pseudo-likelihood

To create the model archetype, we concatenate the data from the fifteen participants and the two conditions to generate a single dataset resulting in four final subsets, two pertaining to LSD condition and two for placebo.

We then estimate the model parameters $\mathbf{J}$ and $\mathbf{h}$ using an approximation to maximum likelihood as described in *Ezaki et al* [24]. Briefly, we find the parameters that maximize the probability of observing the data given the model,

$$(\boldsymbol{h},\boldsymbol{J}) = \underset{\boldsymbol{h},\boldsymbol{J}}{\arg\max}\, \mathcal{L}(\boldsymbol{h},\boldsymbol{J}) = \underset{\boldsymbol{h},\boldsymbol{J}}{\arg\max} \log \mathcal{L}(\boldsymbol{h},\boldsymbol{J}) \tag{3}$$

with

$$\mathcal{L}(\boldsymbol{h},\boldsymbol{J}) = \prod_{t=1}^{t_{\max}} P(\boldsymbol{\sigma}(t)|\boldsymbol{h},\boldsymbol{J}) \tag{4}$$

The likelihood maximum can be found by gradient ascent, with

$$h_i^{\text{new}} = h_i^{\text{old}} + \eta\left(\langle\sigma_i\rangle_{\text{empirical}} - \langle\sigma_i\rangle_{\text{model}}\right) \tag{5}$$

$$J_{ij}^{\text{new}} = J_{ij}^{\text{old}} + \eta\left(\langle\sigma_i\sigma_j\rangle_{\text{empirical}} - \langle\sigma_i\sigma_j\rangle_{\text{model}}\right) \tag{6}$$

where the old/new superscripts refer to the values before and after updating, and with η a small positive constant.

When the number of nodes in the system is large, the calculation of the likelihood from the model because computationally intractable. For this reason, it is approximated by the pseudo-likelihood, a mean-field approximation that approaches the true likelihood as the number of time points goes to infinity [24, 3],

$$\mathcal{L}(\boldsymbol{h},\boldsymbol{J}) = \prod_{t=1}^{t_{\max}} P(\boldsymbol{\sigma}(t)|\boldsymbol{h},\boldsymbol{J}) \approx \prod_{t=1}^{t_{\max}} \prod_{i=1}^{N} \tilde{P}(\sigma_i(t)|\boldsymbol{h},\boldsymbol{J},\boldsymbol{\sigma}_{/i}(t)) \tag{7}$$

with $\tilde{P}(\sigma_i|\boldsymbol{h},\boldsymbol{J},\boldsymbol{\sigma}_{/i})$ the modeled probability distribution for a given spin given the states of all the others, a quantity much easier to compute,

$$\tilde{P}(\sigma_i|\boldsymbol{h},\boldsymbol{J},\boldsymbol{\sigma}_{/i}) = \frac{e^{-\mathcal{H}_i(\boldsymbol{\sigma}|\boldsymbol{h},\boldsymbol{J})}}{\sum_{\sigma_i'} e^{-\mathcal{H}_i(\sigma_i'|\boldsymbol{h},\boldsymbol{J},\boldsymbol{\sigma}_{/i})}} \tag{8}$$

with

$$\mathcal{H}_i(\boldsymbol{\sigma}|\boldsymbol{h},\boldsymbol{J}) = -h_i\,\sigma_i - \sum_{j\neq i\leq N} J_{ij}\sigma_i\sigma_j \tag{9}$$

Using this approximation, the gradient ascent rule becomes

$$h_i^{\text{new}} = h_i^{\text{old}} + \eta\left(\langle\sigma_i\rangle_{\text{empirical}} - \langle\sigma_i\rangle_{\tilde{P}}\right) \tag{10}$$

$$J_{ij}^{\text{new}} = J_{ij}^{\text{old}} + \eta\left(\langle\sigma_i\sigma_j\rangle_{\text{empirical}} - \langle\sigma_i\sigma_j\rangle_{\tilde{P}}\right) \tag{11}$$

where $\langle \sigma_i \rangle_{\tilde{P}}$ and $\langle \sigma_i \sigma_j \rangle_{\tilde{P}}$ are the 1-point and 2-point correlations with respect to distribution $\tilde{P}$ [24],

$$\begin{aligned} \langle \sigma_i \rangle_{\tilde{P}} &= \frac{1}{t_{\max}} \sum_{t=1}^{t_{\max}} \tanh \left[h_i + \sum_{j'=1 j' \neq i}^{N} J_{ij'} \sigma_{j'}(t) \right] \\ \langle \sigma_i \sigma_j \rangle_{\tilde{P}} &= \frac{1}{t_{\max}} \sum_{t=1}^{t_{\max}} \sigma_j(t) \tanh \left[h_i + \sum_{\substack{j'=1 \\ j' \neq i}}^{N} J_{ij'} \sigma_{j'}(t) \right] \end{aligned} \tag{12}$$

Personalization of model — individualized temperature

With $\boldsymbol{h}$ and $\boldsymbol{J}$ fixed in the archetype using the entire dataset, we adapt the archetype model for each subject and condition by changing the model temperature $T = 1/\beta$, that is, by writing

$$P(\boldsymbol{\sigma}|\boldsymbol{h}, \boldsymbol{J}, \beta) = \frac{e^{-\beta \mathcal{H}(\boldsymbol{\sigma}|\boldsymbol{h}, \boldsymbol{J})}}{\sum_{\{\boldsymbol{\sigma}'\}} e^{-\beta \mathcal{H}(\boldsymbol{\sigma}'|\boldsymbol{h}, \boldsymbol{J})}} \tag{13}$$

In this case, the gradient ascent algorithm becomes

$$\beta^{\text{new}} = \beta^{\text{old}} - \eta \left(\langle \mathcal{H} \rangle_{\text{empirical}} - \langle \mathcal{H} \rangle_{\tilde{P}} \right) \tag{14}$$

with a fixed point at $\langle \mathcal{H} \rangle_{\text{empirical}} = \langle \mathcal{H} \rangle_{\tilde{P}}$. This, as in the prior equations, can be seen by taking the derivative of the approximate log-likelihood

$$\log L(\boldsymbol{h}, \boldsymbol{J}) = \sum_{t=1}^{t_{\max}} \log P(\boldsymbol{\sigma}(t)|\boldsymbol{h}, \boldsymbol{J}) = \sum_{t=1}^{t_{\max}} \big(-\beta \mathcal{H}(\boldsymbol{\sigma}(t)|\boldsymbol{h}\boldsymbol{J}) - \log Z(\boldsymbol{h}, \boldsymbol{J}, \boldsymbol{\sigma}_{/i}(t), \beta) \big)$$

with respect to the inverse temperature β, with the partition function given by

$$Z(\boldsymbol{h}, \boldsymbol{J}, \beta, t) = \sum_{\sigma_i'} e^{-\beta \mathcal{H}_i(\sigma_i'|\boldsymbol{h}, \boldsymbol{J}, \boldsymbol{\sigma}_{/i}(t))}$$

The first term becomes the empirical average of the Hamiltonian, and the second the (data dependent) model mean (both up to a constant, since we are not diving by the number of measurements). It can be computed from Equation 12 and from

$$\langle \mathcal{H} \rangle_{\tilde{P}} = -h_i \langle \sigma_i \rangle_{\tilde{P}} - \sum_{j \neq i \leq N} J_{ij} \langle \sigma_i \sigma_j \rangle_{\tilde{P}} \tag{15}$$

Metropolis algorithm and Ising model observables

The Metropolis algorithm is used to compute the observables of the Ising model built from the experimental data. A loop is performed where a random spin is chosen and flipped with a probability $p = \max(1, \exp[-\Delta\mathcal{H}/T])$, where $\Delta\mathcal{H}$ is the change in energy the flipped spin would cause in comparison to the previous configuration and T is the system temperature. This process provides a method to sample the system probability distribution at a given temperature. The method is applied for a sufficient number of iterations to reach steady-state, and the macroscopic variables are obtained as a mean across iterations over a large number of configurations in steady state.

The main global observable is the lattice average magnetization M over the spin lattice S,

$$M = \sum_{i=1}^{N} \sigma_i \tag{16}$$

and lattice energy, where recall N is the number of nodes in the lattice. Magnetic susceptibility and heat capacity can be computed as follows. Let the external field $h_i = h$ be uniform,

$$\mathcal{H}[\sigma] = -\sum_{i<j} J_{ij}\sigma_i\sigma_j - h\sum_j \sigma_j \tag{17}$$

and

$$Z(\beta, h) = \sum_\sigma e^{-\beta\mathcal{H}[\sigma]} \tag{18}$$

be the partition function. The average magnetization is the ensemble average of lattice magnetization,

$$\langle M\rangle = \frac{1}{Z}\sum_\sigma M\, e^{-\beta\mathcal{H}[\sigma]} \tag{19}$$

Then we can express (see, e.g., [57])

$$\langle M\rangle = \frac{1}{\beta Z}\frac{\partial Z}{\partial h} \tag{20}$$

and following similar considerations (with $T = 1/\beta$)

$$\chi = \left.\frac{\partial\langle M\rangle}{\partial B}\right|_T = \sigma_M^2/T, \text{ and } C_v = \left.\frac{\partial\langle\mathcal{H}\rangle}{\partial T}\right|_B = \sigma_{\mathcal{H}}^2/T^2 \tag{21}$$

where the standard deviation computation is taken over the ensemble. We can extend the definition of global to local susceptibility. Let

$$\begin{aligned}
\chi_n &= \left.\frac{\partial\langle M\rangle}{\partial h_n}\right|_T \\
&= \frac{\partial}{\partial h_n}\frac{1}{Z}\sum_\sigma M\, e^{-\beta\mathcal{H}[\sigma]} \\
&= \frac{\beta}{Z}\sum_\sigma M\sigma_n\, e^{-\beta\mathcal{H}[\sigma]} - \frac{\beta}{Z^2}\sum_\sigma M\, e^{-\beta\mathcal{H}[\sigma]}\sum_{\sigma'}\sigma_n\, e^{-\beta\mathcal{H}[\sigma']}
\end{aligned}$$

so

$$\chi_n = \beta\left(\langle M\sigma_n\rangle - \langle M\rangle\langle\sigma_n\rangle\right) \tag{22}$$

In order to smooth the results and deal with slow lattice fluctuations at cold temperatures in finite size systems (the system is bistable for the finite case), we work with modified variables to compute the magnetization and susceptibility statistics using Metropolis generated data. Selection of one of the metastable branches is achieved by flipping, as needed at each sample point, the entire lattice so that the magnetization is positive, $\sigma_n \to \sigma_n\,\mathrm{sign}(M)$. E.g., $M \to |M| = M\,\mathrm{sign}(M)$ for the evaluation of magnetization and global susceptibility (v. Figure 2). Even n-point correlation functions such as $\langle M\sigma_n\rangle$ are invariant. The results away from the critical temperature differ by a constant from the ideal one (the effect is one of smoothing near the critical point) [37].

Statistical analysis

For the analysis of Ising temperatures, in order to compare the results in this repeated measures (within-subject) design, we performed a paired Wilcoxon test (the data is not assumed to be normally distributed) with the temperature estimates. To further test whether the observed increase in temperature under LSD relative to placebo was specific to the architecture parameters h and J, we conducted a non-parametric

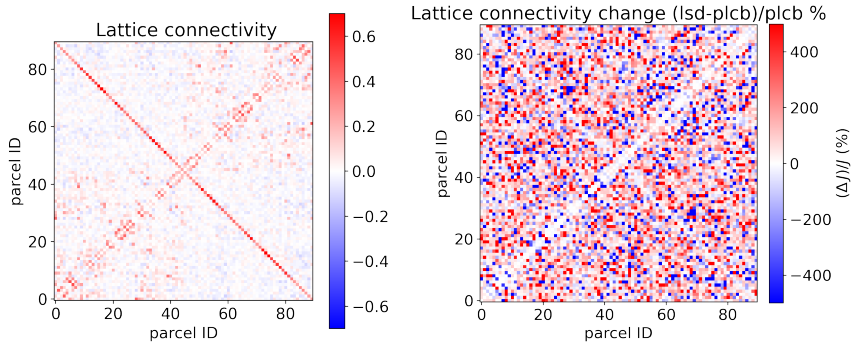

Fig 1. Archetype connectivity. **Left:** the archetype connectivity using all the data. The down-trending diagonal values reflects inter-hemispheric connectivity. **Right:** percent change in connectivity from the placebo dataset archetype to the LSD dataset. By construction, the Ising model (Eq. 1) has zeros in the diagonal elements (i.e. $J_{ii} = 0$).

permutation test on the mean temperature difference [35]. In each permutation (n = 1000), we randomly shuffled the labels of ROIs, and hence the h and J indices of the archetype parameters (see Equation 3). These new set of permuted archetypes (h_p, J_p) were then used to fit the system temperature of each participant and condition (see Equation 13). The null hypothesis is that the measured BOLD activity patterns is drawn from the same probability distribution, regardless of the drug manipulation in which it was recorded. Once the personalized β_p estimates were obtained, we performed the temperature contrast between LSD and placebo. This was done by computing a one-sample t-test for every permutation. The level of statistical significance was estimated by the fraction of t-values derived for every random shuffle that were higher than observed t-values obtained from our original temperature contrast obtained from the non-permuted h and J. Similarly, we performed a paired one-tailed Wilcoxon test with the LZW and BDM complexity estimates.

Results

Archetype connectivity

The first step in our analysis is to identify the parameters h and J that could best fit the fMRI data from all subjects in both conditions — which leads to what we call the 'archetype model.' Additionally, in order to check for network changes due to the effect of LSD, we also estimated the parameters h and J that could best reproduce separately the data from the LSD and placebo conditions separately. Figure 1 shows the resulting connectivity matrix (i.e the values of J_{ij}) estimated from all the data, and also the changes in connectivity between the LSD and placebo conditions.

Between the two archetypes, there was an relative change in the mean connectivity (calculated as $(\bar{J}_{\text{LSD}} - \bar{J}_{\text{placebo}})/\bar{J}_{\text{placebo}}$) of -3.4% (the LSD archetype had slightly weaker weights), with an analogous standard deviation change of -6.7% (the LSD archetype weight distribution had less variance). Analogously, the changes in the mean h array and its standard deviation were respectively -96.3% and -14.5%, reflecting an weaker external drive on the system.

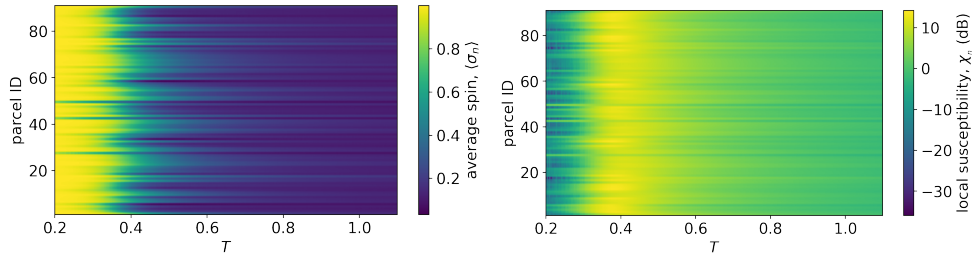

Fig 2. Metropolis runs with archetype model. Local magnetization and susceptibility of the archetype model as a function of temperature.

Archetype phase diagrams

In order to find the critical temperature of the archetype model, we explored its phase space calculating key quantities belonging to the Ising formalism and related measures of signal and algorithmic complexity. Figures 2 and 3 provide, respectively, the local susceptibility and local magnetization at each node in the lattice, and the global magnetization, susceptibility, energy, heat capacity, LZW, and BDM complexity estimates and their standard deviation, as a function of temperature. As can be observed, the critical point (i.e., the peak of the standard susceptibility) is well below $T = 1$, the nominal temperature of the archetype model (which corresponds to the global fit) as well as of the individualized temperatures. This indicates that archetype and individualized models are all in the paramagnetic, supercritical phase. The peaks of susceptibility, heat capacity and LZW variance occur at approximately the same temperature, while BDM complexity variance peaks later. Finally, Figure 2 displays the peak susceptibility of nodes in the parcellation and the temperatures at which they occur. All nodes are above the critical temperature at the nominal temperature of $T = 1$.

Individual temperature shift with LSD

The next step in our analysis was to find two Ising temperatures per subject, characterizing their LSD and placebo conditions. These features can then be compared to the system critical temperature to locate where the temperatures of the two conditions and different subjects sit in the archetype phase space. Figure 4 displays, on the top, personalized temperatures of the fifteen subjects in the LSD and placebo conditions and the temperature difference between conditions for each subject.

Temperatures in the LSD state were found to be substantially higher than in placebo ($6.7\% \pm 5.1\%$; mean $\pm$ standard deviation), with this increase being statistically significant (two-tailed t-test $p = 6.1 \times 10^{-5}$; Cohen's $d = 1.35$). Since Ising temperatures necessarily are not normally distributed, rank-based statistics (one-tailed Wilcoxon test, $p = 9 \times 10^{-5}$) and the non-parametric permutation test shuffling ROI labels in the model yielded highly significant results ($p = 1 \times 10^{-3}$).

LZW and BDM complexity from data and model (synthetic data)

We also extracted features related to the algorithmic complexity both from the empirical fMRI data and the synthetic data generated with the model with the Metropolis algorithm. We would expect these features to show a similar trend to the one obtained with the Ising temperatures. Figures 4 and 5 display the individual LZW and BDM complexity of 15 subjects under the effect of LSD and placebo (left), and the

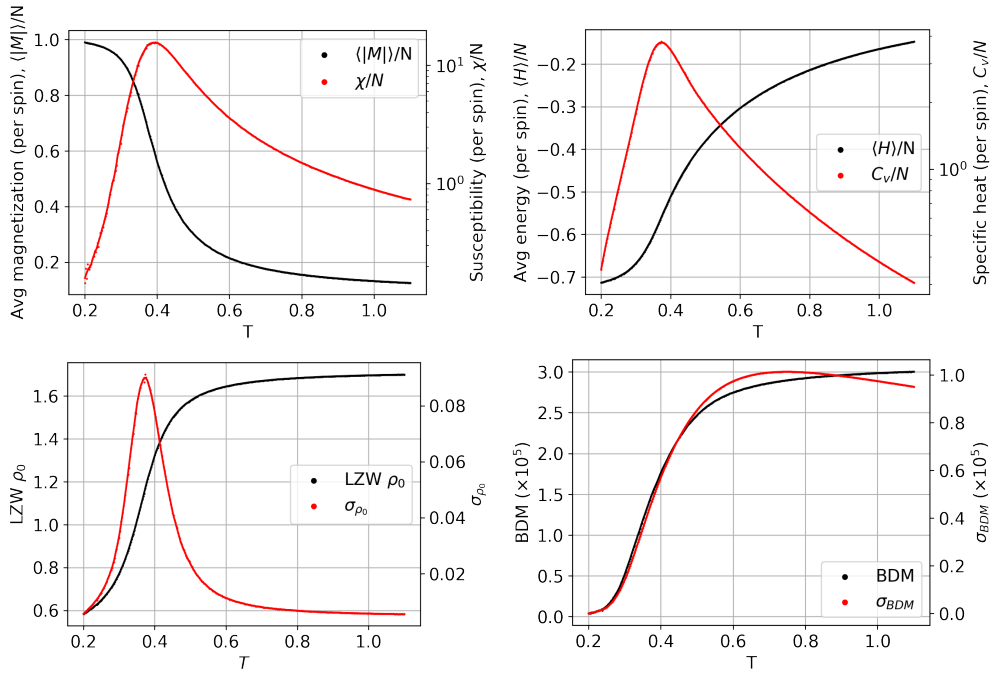

Fig 3. Phase diagram for global archetype model. Top: Global susceptibility and magnetization (left), energy and heat capacity (right). Bottom: LZW complexity (ρ_0) and its standard deviation (left), and BDM complexity and its standard deviation (right), for the archetype model as a function of temperature (the Metropolis algorithm has been run for 10^8 spin flip tests to obtain these plots).

difference in LZW and BDM complexity between the LSD and placebo conditions for each subject (right), calculated respectively with experimental and simulated data using the personalized Ising models.

The LZW complexity in the LSD state from the data was found higher than in the placebo condition for 2/3 of the subjects (Figure 4, middle). The mean and median relative LZW complexity shift with LSD were respectively 0.008 and 0.005, with a standard deviation of 0.013. The paired one-tailed Wilcoxon test with the LZW complexity estimates resulted in $p = 0.04$ for the Wilcoxon test ($p = 0.04$ for the t-test). The probability of finding this or a larger increase of ρ_0 with LSD ingestion was estimated at $p < 0.04$ (one-tailed Wilcoxon test).

As shown in Figure 4 (bottom), the BDM complexity of LSD state from the data is higher for more than 70% of subjects. The mean and median BDM complexity shift with LSD were respectively of 338 and 298, with a standard deviation of 803.6. Also, the BDM complexity from empirical data correlates with the condition ($p = 0.04$, one-tailed Wilcoxon test).

As shown in Figure 5, the increase in LZW and BDM complexity in the LSD state, using synthetic data generated by the personalized models, was statistically significant (one-tailed Wilcoxon test $p = 3.5 \times 10^{-5}$ and $p = 2.1 \times 10^{-4}$, respectively).

We also analyzed the correlation between the features extracted from the data and from the model. A summary of the statistics of the different metrics and the Pearson correlation coefficients between them is given in Tables 1 and 2, whereas the correlation scatter plots can be found in Figure 6 in Appendix B. The difference in LZW and BDM complexity from the model correlates strongly with the delta Ising temperature ($r(13) = 0.91, p = 2.7 \times 10^{-6}$ for LZW and $r(13) = 0.97$, $p = 8.9 \times 10^{-10}$ for BDM). The

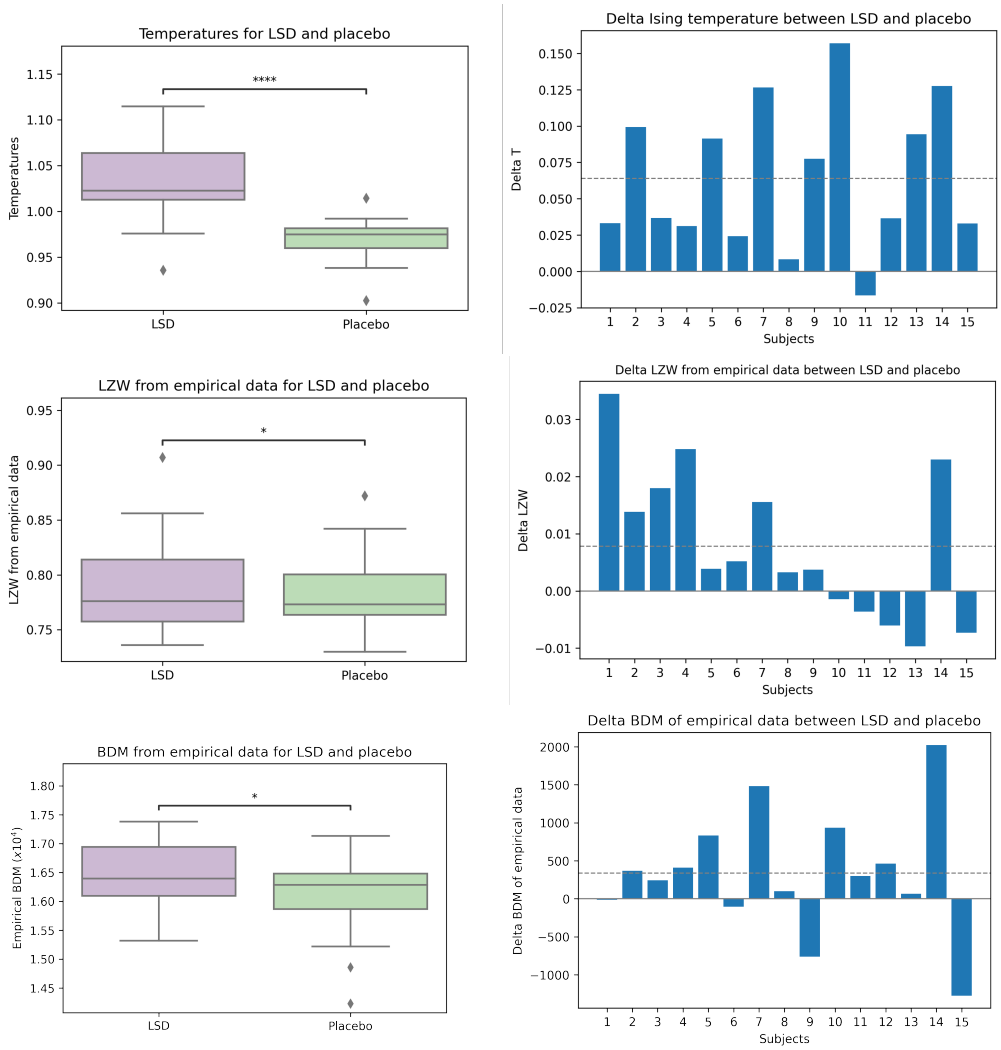

Fig 4. Individual shift of Ising temperature (top), LZW (middle), and BDM (bottom) complexity estimates with LSD using empirical data. Left: Box plots of the metrics of 15 subjects under the effect of LSD and placebo. Right: Bar plot of the metrics differences between LSD and placebo for each subject. The dashed line represents the mean metric. (One star: $p < 0.05$, four stars: $p < 0.0001$)

delta LZW from experimental data does not display a significant relationship with the delta Ising temperature ($r(13) = 0.06, p = 0.83$), nor with the delta LZW complexity from synthetic data ($r(13) = 0.13, p = 0.65$), presumably due to the short length of the time series and limited number of subjects. The difference in BDM complexity from the experimental data correlates with the delta Ising temperature ($r(13) = 0.56, p = 0.03$), whereas it does not show a strong statistical relationship with the delta LZW from the data ($r(13) = 0.35, p = 0.19$), nor with the delta LZW complexity from the model ($r(13) = 0.12, p = 0.42$).

Correlation between questionnaire scores and data features

In the LSD trial, participants were asked to answer two types of questionnaires to give feedback on their psychedelic experience. They completed VAS-style ratings via

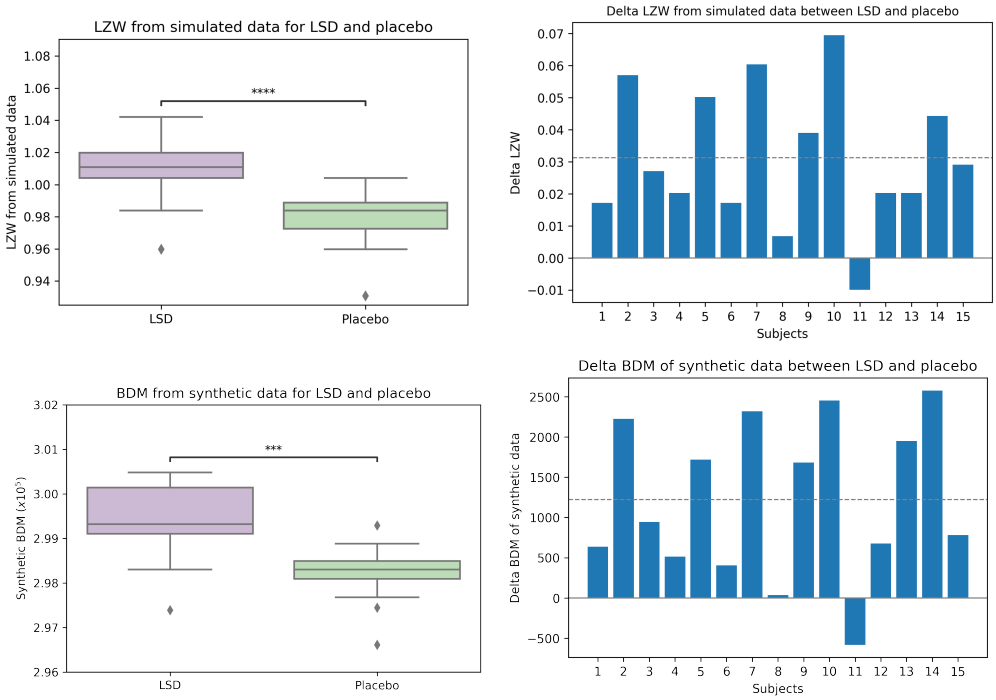

Fig 5. Individual shift of LZW (top) and BDM (bottom) complexity estimates with LSD using synthetic data. Left: Box plots of the metrics of 15 subjects under the effect of LSD and placebo. Right: Bar plot of the metrics differences between LSD and placebo for each subject. The dashed line represents the mean metric. (Three stars: $p < 0.001$, four stars: $p < 0.0001$)

	Median (%)	Mean (%)	t-score	p-value (one-tailed)
Ising T	3.76	6.61	4.93	9×10^{-5}
LZW data	0.50	1.00	2.30	0.04
LZW synth	2.75	3.20	5.56	9×10^{-5}
BDM data	1.83	2.10	1.63	0.04
BDM synth	0.32	0.41	4.86	2×10^{-4}

Table 1. Summary statistics of different metrics. All metrics refer to the change of variable (LSD-Placebo).

Pearson cc	Ising T	LZW data	LZW synth	BDM data	BDM synth
Ising T		0.06	0.91****	0.56*	0.97****
LZW data			0.13	0.35	0.12
LZW synth				0.12	0.90****
BDM data					0.49

Table 2. Pearson correlation between different metrics.

button-press and a digital display screen after each scan and the 11-factor altered states of consciousness (ASC) questionnaire at the end of each dosing day [8]. The most important ASC scores reported by the authors were elementary imagery ("I saw regular patterns in complete darkness or with closed eyes.", "I saw colors before me in total darkness or with closed eyes.", "I saw lights or flashes of light in total darkness or with closed eyes."), complex imagery ("I saw scenes rolling by in total darkness or with my

eyes closed.", "I could see pictures from my past or fantasy extremely clearly.", "My imagination was extremely vivid."), and audio-video synesthesia ("Noises seemed to influence what I saw.", "The shapes of things seemed to change by sounds and noises.", "The colors of things seemed to be changed by sounds and noises.").

We calculated the questionnaire scores difference between the LSD and placebo sessions for each category. Then, we computed the average scores of each questionnaire to have a single measure of the overall intensity of the subjective experience. We checked the Pearson correlation between the subjects' questionnaire scores and the features extracted from the data, i.e., Ising temperature, LZW, and BDM from experimental data.

Tables 4 and 5 in Appendix D provide the questionnaire scores for all subjects, their average, and the Pearson correlation coefficients between the scores and the features extracted from the data.

No strong statistical relationships were seen between the subjective reports and the features. However, trends were observed between complex imagery and Ising temperatures ($r = 0.42$) and elementary imagery and LZW complexity ($r = 0.48$), both obtained from the ASC questionnaire. From the VAS-style ratings, trends were observed between emotional arousal and all three features (positive trends for Ising temperatures and BDM complexity, whereas negative ones with LZW complexity).

Discussion

We have developed here a framework for the generation of personalized Ising models starting from archetypes, where data from multiple subjects are assimilated.

With regard to the archetypes built separately in each condition, the main changes between the global LSD and placebo archetypes were a decrease of mean connectivity and connectivity variance in the LSD group, as well as a stronger decrease in the external coupled field h_i (which is essentially null in the LSD archetype). Both features suggest a loosening of the network towards disorder with the ingestion of LSD, in a manner consistent with the rest of the analysis.

We found it especially useful to generate a global archetype assimilating the data from all participants and conditions. This is convenient first because of the relative scarcity of data produced by fMRI BOLD sequences and, second, because it provides a common framework for comparison of individualized models (in this case, characterized by their temperatures relative to the archetype). The archetype generates behavior as a function of temperature similar to the standard, nearest-neighbor Ising model, with a clearly defined critical point. However, unlike the original Ising model, this model does not display translational symmetry because the model parameters (J_{ij} and h_i) vary with each parcel. As a consequence, some of the nodes of the archetype model display higher sensitivity to perturbations than others. The brain parcels corresponding to these nodes are natural areas for further study of the effects of stimulation (invasive or non-invasive) in more sophisticated computational brain models [19, 69].

With regard to the personalized temperatures, we found a very strong correlation between individualized temperature and condition. The individualized temperatures derived from fMRI BOLD data almost uniformly increased with the LSD condition relative to placebo. Statistically speaking, the results are very robust. Moreover, both the archetype temperature ($T = 1$) and the individualized ones for both conditions were found to be above the critical point of the model. The state in all cases was found to be in the paramagnetic phase, as was found in Ezaki et al (2020) [23].

Since Ising temperature was expected to correlate with entropy and disorder in the models, and because of the relevance of the notion of complexity in the analysis of brain data, we studied two proxies (upper bounds) of algorithmic complexity, one closely

related to Shannon entropy (LZW), the other more directly connected with the concept of Kolmogorov complexity (BDM). We did this first starting from the data itself and, then, also working with synthetic data generated from the personalized Ising models. While complexity metrics derived from the data related weakly (but significantly) with temperature and condition presumably due to the limited number of data per participant and condition, model-derived LZW and BDM complexity estimates—which are monotonic functions of temperature (Figure 3 and 5)—also correlated strongly with condition.

Figure 3 (bottom right) displays the monotonic behavior of BDM complexity with respect to temperature, with a very sharp increase and then almost a plateau. This suggests the bound on complexity magnitude, whereas the slope of increase should be correlated with model parameters and describing the simulation condition. The BDM calculation was time-consuming due to size of the matrices involved, but it has opened an avenue to further investigate the slope of the curve and see if it can be used to get more insight from empirical data and also design better simulations. One limitation in the BDM calculation is that, as the size of matrices is increasing, BDM gets gradually closer and closer to an entropy measurement, as we use precomputed CTM for smaller matrices. Moreover, it is important to note that, in our complexity analysis, we are bounded to binary data, which makes the analysis dependent on how meaningful the binarized version of the data is.

Overall, our results are consistent with the notion that psychedelics drive brain dynamics into a more disordered state and, in our modeling framework, away from criticality. The RElaxed Beliefs Under pSychedelics (REBUS) framework [4]) addresses the phenomenology and physiology of psychedelic states by integrating mechanistic insights with the free-energy principle (FEP, [26, 55]). The FEP is a formulation based on causal statistical theory that accounts for action, perception, and learning, and the entropic brain hypothesis (EBH [5]), which associates entropy of spontaneous brain activity with the richness (vividness and diversity) of subjective experience (and posits that psychedelics increase both).

The mechanisms of action of psychedelics are believed to begin with stimulation of a specific serotonin receptor subtype (5-HT2AR) on cortical layer V pyramidal neurons, i.e., this is the control signal that results in increased neuronal excitability and dysregulated cortical population-level activity [54]. Through this action, psychedelics are believed to disrupt the regular functioning of various high-level system properties — e.g., major cortical oscillatory rhythms and the integrity of large-scale networks — that are hypothesized to encode the precision-weighting of internal models — i.e., priors, beliefs, or assumptions. According to the so-called 'REBUS' model [4], psychedelics disrupt models sitting atop the modeling hierarchy, with direct consequences on experience. Interference with microcircuitry associated with high-level models may be expected to release lower-level models that would otherwise be suppressed.

In [67], we hypothesized that increased apparent (Shannon) complexity (entropy) of spontaneous activity is a logical corollary of this action, as courser grain functional architecture will become finer-grained, which is indeed observed using measures such as LZW [70], such as LZW [65]. The present study extends on previous work, however, by incorporating algorithmically-oriented methods such as BDM. Our results agree with earlier work pointing to the usefulness of complexity metrics and the hypothesis that signal complexity should increase with increased system temperature, and that psychedelics should increase both [64].

As discussed in the context of the algorithmic information theory of consciousness (KT) [64, 67], psychedelics will shift the dynamics of an agent system tracking world data to a less constrained state further away from criticality, and hence produce more complex signals.

The above is in line with the idea that the brain operates near a critical point (v. [62, 32, 83] and references therein), and that psychedelics move dynamics into a more disordered state [4]. However, at least in our model and as already described in previous work using similar methods [24, 23], we found that in our cohort the resting brain in the placebo condition is already above the critical point—that is, the resting, wakeful brain is in a supercritical state as observed through the Ising framework lens. This is consistent with the idea that, while mutual information peaks at the critical temperature, information flow in such systems peaks in the disordered (paramagnetic) phase [2], which is in apparent contradiction with other studies suggesting a subcritical nature of healthy brain dynamics [4]. We note here in passing that the term "criticality" is used differently by different authors, e.g., dynamical vs. statistical criticality, whose relation is the subject of current research [83]. At least with the data in this study, the statistical criticality metrics developed here — the supercritical system temperature of an Ising model—, provided the best correlate of experimental condition. Finally, with regard to the relation of these metrics with subjective experience as measured by questionnaires, some weak correlations were found at the trend level with all metrics (temperature and complexity metrics), presumably because of the limited number of data and the inherent heterogeneity of self-reports and that these particular ratings were done post-hoc without precise reference to the scanning periods.

Conclusions

In this paper we have studied criticality features of brain dynamics under LSD in a within-subject study using the Ising model formalism and algorithmic complexity using Lempel-Ziv and the Block Decomposition methods. Personalized Ising models were created using fMRI BOLD data by adjusting the model temperature for each subject and condition in relation to the group average model. We found that the effects of LSD translate into increased BOLD signal complexity and Ising temperature, in agreement with earlier findings and predictions from existing theories of the effects of psychedelics such as the relaxed beliefs under psychedelics (REBUS), the anarchic brain hypothesis [4], and the algorithmic information theory of consciousness (KT) [64, 67]. More precisely, in agreement with earlier work [23], we found that the system in the placebo condition was already in the paramagnetic phase—above the critical point—, with ingestion of LSD resulting in a shift away from criticality into a more disordered state. These results must be interpreted with care, as the Ising framework used here provides a simple one-parameter model for fitting the individual data. Other studies, using different methods, suggest that LSD shifts system dynamics closer to criticality [1, 78], while, for example, using similar methods to ours, higher fluid intelligence has been associated with closer to critical resting-state neural dynamics [23]. Further work is needed to reconcile these results, which may stem from modeling choices and criticality metrics [76].

A List of AAL areas

Here we report the list of AAL areas in the specific order they were used in this study (Table 3).

Table 3. Regions of interest from AAL atlas. The AAL areas were ordered in the following way: first all the areas in the left hemisphere (LH), and then all the areas in the right hemisphere (RH) in reverse order, so that they are "symmetrized" with respect to the contralateral hemisphere.

idx	ROI name		idx	ROI name	
1	Precentral	LH	46	Temporal_Inf	RH
2	Frontal_Sup	LH	47	Temp_Pole_Mid	RH
3	Frontal_Sup_Orb	LH	48	Temporal_Mid	RH
4	Frontal_Mid	LH	49	Temp_Pole_Sup	RH
5	Frontal_Mid_Orb	LH	50	Temporal_Sup	RH
6	Frontal_Inf_Oper	LH	51	Heschl	RH
7	Frontal_Inf_Tri	LH	52	Thalamus	RH
8	Frontal_Inf_Orb	LH	53	Pallidum	RH
9	Rolandic_Oper	LH	54	Putamen	RH
10	Supp_Motor	LH	55	Caudate	RH
11	Olfactory	LH	56	Paracentral_Lob	RH
12	Frontal_Sup_Med	LH	57	Precuneus	RH
13	Frontal_Med_Orb	LH	58	Angular	RH
14	Rectus	LH	59	SupraMarginal	RH
15	Insula	LH	60	Parietal_Inf	RH
16	Cingulum_Ant	LH	61	Parietal_Sup	RH
17	Cingulum_Mid	LH	62	Postcentral	RH
18	Cingulum_Post	LH	63	Fusiform	RH
19	Hippocampus	LH	64	Occipital_Inf	RH
20	ParaHippo	LH	65	Occipital_Mid	RH
21	Amygdala	LH	66	Occipital_Sup	RH
22	Calcarine	LH	67	Lingual	RH
23	Cuneus	LH	68	Cuneus	RH
24	Lingual	LH	69	Calcarine	RH
25	Occipital_Sup	LH	70	Amygdala	RH
26	Occipital_Mid	LH	71	ParaHippo	RH
27	Occipital_Inf	LH	72	Hippocampus	RH
28	Fusiform	LH	73	Cingulum_Post	RH
29	Postcentral	LH	74	Cingulum_Mid	RH
30	Parietal_Sup	LH	75	Cingulum_Ant	RH
31	Parietal_Inf	LH	76	Insula	RH
32	SupraMarginal	LH	77	Rectus	RH
33	Angular	LH	78	Frontal_Med_Orb	RH
34	Precuneus	LH	79	Frontal_Sup_Med	RH
35	Paracentral_Lob	LH	80	Olfactory	RH
36	Caudate	LH	81	Supp_Motor	RH
37	Putamen	LH	82	Rolandic_Oper	RH
38	Pallidum	LH	83	Frontal_Inf_Orb	RH
39	Thalamus	LH	84	Frontal_Inf_Tri	RH
40	Heschl	LH	85	Frontal_Inf_Oper	RH
41	Temporal_Sup	LH	86	Frontal_Mid_Orb	RH
42	Temp_Pole_Sup	LH	87	Frontal_Mid	RH
43	Temporal_Mid	LH	88	Frontal_Sup_Orb	RH
44	Temp_Pole_Mid	LH	89	Frontal_Sup	RH
45	Temporal_Inf	LH	90	Precentral	RH

B Correlation between metrics

We checked the correlation between features extracted from data as shown in Figure 6.

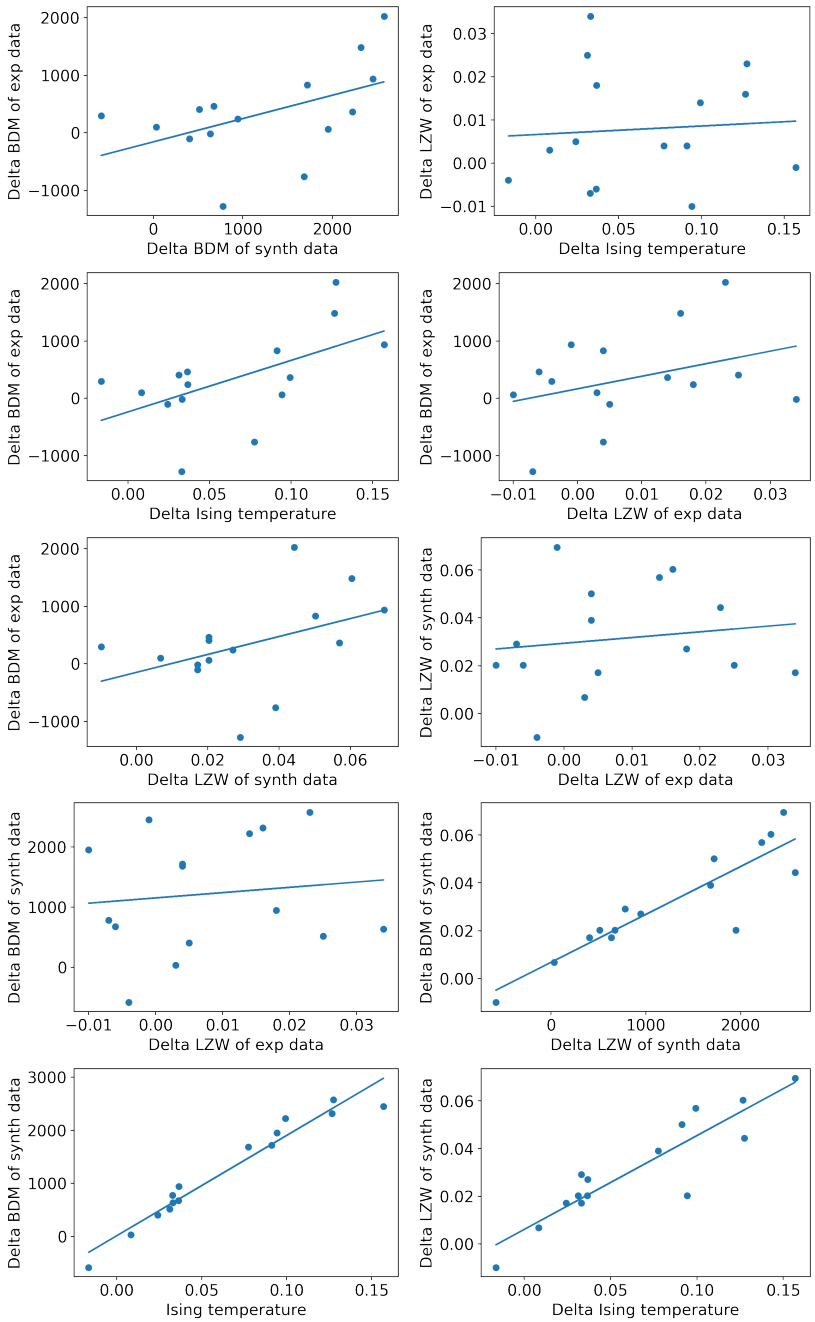

Fig 6. Correlation scatter plots between the metrics. Correlation plots between the metrics, i.e., delta LZW complexity of the simulated and empirical data, delta Ising temperature, and delta BDM complexity of the simulated and empirical data.

C Subjects questionnaire scores and their correlation with metrics

Difference between LSD and placebo												
Subjects	Unity	Spirit	Bliss	Insight	Disem	Cont&Cog	Anxiety	Complex	Element	Aud/Vis	Meaning Perc	Average
1	0.0	0.0	0.0	0.0	0.1	0.0	0.0	0.1	1.0	0.3	0.0	0.1
2	0.4	0.2	0.4	0.4	0.5	0.2	0.0	0.6	0.6	0.7	0.3	0.4
3	0.0	0.2	0.1	0.3	0.0	0.2	0.1	0.1	0.2	0.2	0.2	0.1
4	0.8	0.3	1.0	0.8	1.0	0.6	0.5	0.7	1.0	0.9	0.5	0.7
5	0.0	0.0	0.0	0.0	0.0	0.0	0.0	0.0	0.0	0.0	0.0	0.0
6	0.2	0.0	0.3	0.5	0.7	0.0	0.0	0.5	1.0	0.7	0.5	0.4
7	0.2	0.1	0.1	0.1	0.7	0.6	0.3	0.4	1.0	0.0	0.2	0.3
8	0.1	0.2	0.2	0.1	0.0	0.1	0.0	0.2	0.6	0.1	0.0	0.1
9	0.2	0.0	0.0	0.0	0.0	0.1	0.0	0.5	1.0	1.0	0.0	0.2
10	0.2	0.3	0.2	0.5	0.0	0.2	0.3	0.8	0.9	0.9	0.3	0.4
11	0.2	0.1	0.3	0.2	0.5	0.3	0.1	0.4	0.6	0.3	0.2	0.3
12	0.7	0.6	0.5	0.3	0.3	0.0	-0.1	0.5	0.2	0.0	0.7	0.3
13	0.4	0.3	0.3	0.2	0.3	0.2	0.0	0.2	0.5	0.6	0.5	0.3
14	0.4	0.3	0.3	0.3	0.5	0.5	0.2	1.0	1.0	1.0	0.9	0.6
15	0.5	0.5	0.6	0.5	0.3	0.4	0.1	0.5	0.4	0.9	0.7	0.5
Ising cc	-0.07	0.06	-0.21	-0.10	-0.10	0.23	0.26	0.42	0.19	0.27	0.11	0.14
LZW cc	-0.13	-0.37	0.00	0.00	0.19	0.26	0.38	0.03	0.48	0.01	-0.10	0.11
BDM cc	-0.02	-0.03	-0.09	-0.10	0.20	0.38	0.40	0.34	0.17	-0.19	0.17	0.13

Table 4. ASC questionnaire scores and their correlation with features extracted from data. The higher scores are colored in darker yellow, whereas Pearson correlation coefficients higher in absolute value than 0.30 are colored in blue. Full names of ASC questionnaire categories: Experience of unity, Spiritual experience, Blissful state, Insightfulness, Disembodiment, Impaired control and cognition, Anxiety, Complex imagery, Elementary imagery, Audio-visual synesthesiae, Changed meaning of percepts.

Average difference between LSD and placebo for session 1 and 2							
Subject	Intensity	Simple	Complex	Emotional Arousal	Positive Mood	Ego Dissolution	Average
1	11	16	11	3	10	0	8
2	12	10	7	12	4	16	10
3	11	5	1	3	2	0	3
4	13	20	20	11	10	2	13
5	9	0	1	12	-1	0	4
6	15	17	17	6	10	6	12
7	11	1	1	12	0	1	4
8	9	6	3	10	1	0	5
9	4	4	0	5	7	0	3
10	13	11	3	10	0	0	6
11	11	9	10	10	12	3	9
12	19	15	12	19	19	20	17
13	15	10	4	15	5	11	10
14	19	19	19	18	17	17	18
15	15	5	6	14	8	11	10
Ising cc	0.10	-0.15	-0.26	0.31	-0.33	0.11	-0.07
LZW cc	-0.07	0.34	0.35	-0.38	0.06	-0.22	0.05
BDM cc	0.31	0.15	0.19	0.39	0.02	0.11	0.22

Table 5. VAS questionnaire scores and their correlation with features extracted from data. The higher scores are colored in darker yellow, whereas Pearson correlation coefficients higher in absolute value than 0.30 are colored in blue.

D Comparison with 5-HT$_{2A}$ receptors map

As the LSD effects seem to be related to the density of the 5-HT$_{2A}$ receptors, we checked the correlation between the receptor density in the brain and the changes in the archetype parameters obtained separately from the LSD and placebo data. The 5-HT$_{2A}$ receptors map in AAL parcellation was obtained from Deco et al. (2018) [21]. Figure 7 displays the relation between the archetype changes from LSD to placebo and the 5-HT$_{2A}$ receptor density. No statistically significant trends were observed.

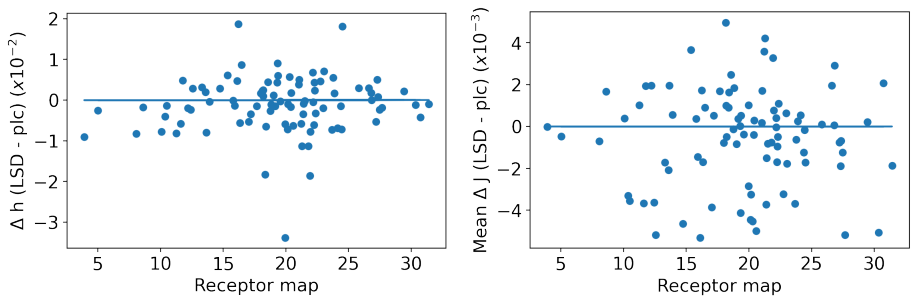

Fig 7. Correlation scatter plots between the archetype changes from LSD to placebo and the 5-HT$_{2A}$ receptor density. Correlation between the archetype changes from LSD to placebo and the 5-HT$_{2A}$ receptor density in the 90 AAL parcels. The mean connectivity J per parcel was obtained by averaging the connectivity difference of one parcel with all the others ($J_i = (1/N_p)\sum_j J_{ij}$).

Acknowledgments

GR, GiD, DL-S, ND have received funding from the European Research Council (ERC Synergy Galvani) under the European Union's Horizon 2020 research and innovation programme (grant agreement No 855109) and under European Union's Horizon 2020 research and innovation programme under grant agreement No 101017716 (Neurotwin). RLC-H is supported by the Ralph Metzner Distinguished Professorship endowment. GuD is supported by the ERC Advanced Grant DYSTRUCTURE (295129), the Spanish Research Project PSI2016-75688-P, the European Union's Horizon 2020 Framework Programme for Research and Innovation under the Specific Grant Agreement No. 785907 (Human Brain Project SGA2), and the European Union's Horizon 2020 research and innovation programme (grant agreement No 855109). NAK has received funding from the European Union under the Horizon 2020 programme (MultipleMS grant agreement 733161 and DECISION Grant agreement 847949). FR is supported by the Ad Astra Chandaria foundation. AP-A was supported by the Human Brain Project SGA3 (945539).

Data and code availability

Code for Ising modeling can be found at `https://github.com/giulioruffini/LSD_Ising_project`, and for LZW analysis at `https://github.com/giulioruffini/StarLZW`. The code for fMRI analysis is available at `https://github.com/decolab/cb-neuromod`. The multimodal neuroimaging data from the experiment is available upon request from (contact Dr. Robin Carhart-Harris). BDM calculation code in different languages are available on

the algorithm dynamics lab website, software page, https://www.algorithmicdynamics.net/software.html.

Contributions

GR: conceptualization, methodology, software, writing original manuscript; GiD: data processing, software, manuscript contributions; DLS: statistical analysis support; ND: conceptualization, software, data processing; FER: manuscript revision, conceptualization; NAK: data analysis, conceptualization, manuscript revision; APA: conceptualization; MLK: data processing; RC-H: experimental conceptualization, data collection, manuscript revision; GuD: conceptualization, manuscript revision.

References

[1] Selen Atasoy et al. "Connectome-harmonic decomposition of human brain activity reveals dynamical repertoire re-organization under LSD". en. In: *Sci. Rep.* 7.1 (Dec. 2017), p. 17661.

[2] Lionel Barnett et al. "Information flow in a kinetic Ising model peaks in the disordered phase". en. In: *Phys. Rev. Lett.* 111.17 (Oct. 2013), p. 177203.

[3] J. Besag. "Statistical analysis of non-lattice data". In: *J. R. Stat. Soc. D* 25 (1975), pp. 179–195.

[4] R. L. Carhart-Harris and K. J. Friston. "REBUS and the Anarchic Brain: Toward a Unified Model of the Brain Action of Psychedelics". In: *Pharmacological Reviews* 71.3 (July 2019), pp. 316–344.

[5] RL Carhart-Harris. "The entropic brain — revisited". In: *Neuropharmacology* 142.167–178 (2018).

[6] Robin L Carhart-Harris et al. "Neural correlates of the psychedelic state as determined by fMRI studies with psilocybin". en. In: *Proc. Natl. Acad. Sci. U. S. A.* 109.6 (Feb. 2012), pp. 2138–2143.

[7] Robin L Carhart-Harris et al. "The entropic brain: a theory of conscious states informed by neuroimaging research with psychedelic drugs". en. In: *Front. Hum. Neurosci.* 8 (Feb. 2014), p. 20.

[8] Robin L. Carhart-Harris et al. "Neural correlates of the LSD experience revealed by multimodal neuroimaging". In: *Proceedings of the National Academy of Sciences* 113.17 (2016), pp. 4853–4858. ISSN: 0027-8424. DOI: 10.1073/pnas.1518377113. eprint: https://www.pnas.org/content/113/17/4853.full.pdf. URL: https://www.pnas.org/content/113/17/4853.

[9] Dante R Chialvo. "Emergent complex neural dynamics". en. In: *Nat. Phys.* 6.10 (Oct. 2010), pp. 744–750.

[10] Dante R. Chialvo. "Critical brain networks". In: *Physica A* 340 (2004), pp. 756–765.

[11] Kim Christensen and Nicholas R Moloney. *Complexity and criticality*. London, England: Imperial College Press, 2005.

[12] Filippo Cieri et al. "Brain Entropy During Aging Through a Free Energy Principle Approach". In: *Frontiers in Human Neuroscience* 15 (2021), p. 139. ISSN: 1662-5161. DOI: 10.3389/fnhum.2021.647513. URL: https://www.frontiersin.org/article/10.3389/fnhum.2021.647513.

[13] Luca Cocchi et al. "Criticality in the brain: A synthesis of neurobiology, models and cognition". en. In: *Prog. Neurobiol.* 158 (Nov. 2017), pp. 132–152.

[14] Thomas M. Cover and Joy A. Thomas. *Elements of information theory.* 2nd ed. John Wiley & sons, 2006.

[15] Gemma De las Cuevas and Toby S. Cubitt. "Simple universal models capture all classical spin physics". In: *Science* 351.6278 (2016).

[16] T.K. Das et al. "Highlighting the Structure-Function Relationship of the Brain with the Ising Model and Graph Theory". In: *BioMed Research International* 237898 (2014).

[17] G Deco et al. "Whole-Brain Multimodal Neuroimaging Model Using Serotonin Receptor Maps Explains Non-linear Functional Effects of LSD". In: *Curr Biol.* 28.19 (2018), pp. 3065–3074.

[18] Gustavo Deco and Viktor K Jirsa. "Ongoing cortical activity at rest: criticality, multistability, and ghost attractors". en. In: *J. Neurosci.* 32.10 (Mar. 2012), pp. 3366–3375.

[19] Gustavo Deco and Morten L. Kringelbach. "The economy of anatomy: Discovering the turbulent homogeneous isotropic functional core organisation of the human brain". In: *bioRxiv* (2019).

[20] Gustavo Deco et al. "Key role of coupling, delay, and noise in resting brain fluctuations". In: *Proceedings of the National Academy of Sciences* 106.25 (2009), pp. 10302–10307. ISSN: 0027-8424. DOI: `10.1073/pnas.0901831106`. URL: `http://www.pnas.org/content/106/25/10302`.

[21] Gustavo Deco et al. "Perturbation of whole-brain dynamics in silico reveals mechanistic differences between brain states". In: *NeuroImage* 169 (2018), pp. 46–56. ISSN: 1053-8119. DOI: `https://doi.org/10.1016/j.neuroimage.2017.12.009`. URL: `http://www.sciencedirect.com/science/article/pii/S1053811917310236`.

[22] E Erten et al. "Criticality and information dynamics in epidemiological models". In: *Entropy (Basel)* 19.5 (Apr. 2017), p. 194.

[23] Takahiro Ezaki et al. "Closer to critical resting-state neural dynamics in individuals with higher fluid intelligence". en. In: *Commun. Biol.* 3.1 (Feb. 2020), p. 52.

[24] Takahiro Ezaki et al. "Energy landscape analysis of neuroimaging data". In: *Philos Trans R Soc A* 375.20160287 (2017).

[25] Daniel Fraiman et al. "Ising-like dynamics in large-scale functional brain networks". en. In: *Phys. Rev. E Stat. Nonlin. Soft Matter Phys.* 79.6 Pt 1 (June 2009), p. 061922.

[26] Karl Friston. "The free-energy principle: a unified brain theory?" en. In: *Nat. Rev. Neurosci.* 11.2 (Feb. 2010), pp. 127–138.

[27] Peter Gasser, Katharina Kirchner, and Torsten Passie. "LSD-assisted psychotherapy for anxiety associated with a life-threatening disease: a qualitative study of acute and sustained subjective effects". en. In: *J. Psychopharmacol.* 29.1 (Jan. 2015), pp. 57–68.

[28] Mark A Geyer and Franz X Vollenweider. "Serotonin research: contributions to understanding psychoses". en. In: *Trends Pharmacol. Sci.* 29.9 (Sept. 2008), pp. 445–453.

[29] Nigel Goldenfeld. *Lectures on Phase Transitions and the Renormalization Group.* London, England: Addison Wesley, Dec. 1991.

[30] Roland R Griffiths et al. "Psilocybin produces substantial and sustained decreases in depression and anxiety in patients with life-threatening cancer: A randomized double-blind trial". en. In: *J. Psychopharmacol.* 30.12 (Dec. 2016), pp. 1181–1197.

[31] M. Gu and A. Perales. "Encoding universal computation in the ground states of Ising lattices". In: *Phys. Rev. E* 86.011116 (2012), pp. 1–6.

[32] Ariel Haimovici et al. "Brain organization into resting state networks emerges at criticality on a model of the human connectome". en. In: *Phys. Rev. Lett.* 110.17 (Apr. 2013), p. 178101.

[33] Fran Hancock et al. "May the 4c's be with you: An overview of complexity-inspired frameworks for analyzing resting-state neuroimaging data". Mar. 2022.

[34] Janina Hesse and Thilo Gross. "Self-organized criticality as a fundamental property of neural systems". In: *Frontiers in Systems Neuroscience* 8 (2014). ISSN: 1662-5137. DOI: 10.3389/fnsys.2014.00166. URL: https://www.frontiersin.org/article/10.3389/fnsys.2014.00166.

[35] Andrew P Holmes et al. "Nonparametric analysis of statistic images from functional mapping experiments". In: *Journal of Cerebral Blood Flow & Metabolism* 16.1 (1996), pp. 7–22.

[36] J. J. Hopfield. "Neural networks and physical systems with emergent collective computational abilities". In: *PNAS* 79 (1982), pp. 2554–2558.

[37] Eduardo Ibarra-Garcıa-Padilla, Carlos Gerardo Malanche-Flores, and Freddy Jackson Poveda-Cuevas. "The hobbyhorse of magnetic systems: the Ising model". In: *Eur. J. Phys.* 37.6 (Nov. 2016), p. 065103.

[38] E.T. Jaynes. "Information theory and statistical mechanics". In: *Physical Review* 106.4 (1957), pp. 620–630.

[39] E.T. Jaynes. *Probability theory - the logic of science*. Cambridge, 2003.

[40] Henrik Jeldtoft Jensen. *Self-Organized Criticality: Emergent Complex Behavior in Physical and Biological Systems*. Cambridge Lecture Notes in Physics. Cambridge University Press, 1998. DOI: 10.1017/CBO9780511622717.

[41] Matthew W Johnson et al. "Classic psychedelics: An integrative review of epidemiology, therapeutics, mystical experience, and brain network function". en. In: *Pharmacol. Ther.* 197 (May 2019), pp. 83–102.

[42] F. Kaspar and H. G. Schuster. "Easily calculable measure for the complexity of spatiotemporal patterns". In: *Phys. Rev. A* 36.2 (1987), pp. 842–848.

[43] T. Kohler and T. Cubitt. "Translationally Invariant Universal Classical Hamiltonians". In: *Journal of Statistical Physics* 176 (2019), pp. 228–261.

[44] Teri S Krebs and Pål-Ørjan Johansen. "Lysergic acid diethylamide (LSD) for alcoholism: meta-analysis of randomized controlled trials". en. In: *J. Psychopharmacol.* 26.7 (July 2012), pp. 994–1002.

[45] A Lempel and J Ziv. "On the complexity of finite sequences". In: *IEEE Transactions on Information Theory* IT-22.1 (Jan. 1976), pp. 75–81.

[46] Roger Lewin. *Complexity*. en. 2nd ed. Chicago, IL: University of Chicago Press, Dec. 1992.

[47] Mike Li et al. "Transitions in information processing dynamics at the whole-brain network level are driven by alterations in neural gain". In: *PLOS Computational Biology* 15.10 (2019), pp. 1–27. DOI: 10.1371/journal.pcbi.1006957. URL: https://doi.org/10.1371/journal.pcbi.1006957.

[48] M A McCall, D G Tieman, and H V Hirsch. "Chronic intraventricular administration of lysergic acid diethylamide (LSD) affects the sensitivity of cortical cells to monocular deprivation". en. In: *Brain Res.* 250.2 (Nov. 1982), pp. 301–308.

[49] Drummond E-Wen McCulloch et al. "Psychedelic resting-state neuroimaging: A review and perspective on balancing replication and novel analyses". en. In: *Neurosci. Biobehav. Rev.* 104689 (May 2022), p. 104689.

[50] Pedro A M Mediano and Murray Shanahan. "Balanced information storage and transfer in modular spiking neural networks". In: (Aug. 2017). arXiv: `1708.04392 [q-bio.NC]`.

[51] Pedro A M Mediano et al. "Integrated information as a common signature of dynamical and information-processing complexity". In: *Chaos* 32.1 (Jan. 2022), p. 13115.

[52] F Müller et al. "Increased thalamic resting-state connectivity as a core driver of LSD-induced hallucinations". en. In: *Acta Psychiatr. Scand.* 136.6 (Dec. 2017), pp. 648–657.

[53] Ernst Niebur and Dietmar Plenz, eds. *Criticality in Neural Systems*. en. Annual Reviews of Nonlinear Dynamics and Complexity (VCH). Weinheim, Germany: Wiley-VCH Verlag, Apr. 2014.

[54] David Nutt, David Erritzoe, and Robin Carhart-Harris. "Psychedelic psychiatry's brave new world". en. In: *Cell* 181.1 (Apr. 2020), pp. 24–28.

[55] Thomas Parr. *Active inference : the free energy principle in mind, brain, and behavior*. Cambridge, Massachusetts: The MIT Press, 2022. ISBN: 0262045354.

[56] Torsten Passie et al. "The pharmacology of lysergic acid diethylamide: a review". en. In: *CNS Neurosci. Ther.* 14.4 (2008), pp. 295–314.

[57] R.K. Pathria and P. D. Beale. *Statistical Mechanics*. Elsevier Ltd, 2011.

[58] Dietmar Plenz et al. "Self-Organized Criticality in the Brain". In: *Frontiers in Physics* 9 (2021). ISSN: 2296-424X. DOI: `10.3389/fphy.2021.639389`. URL: `https://www.frontiersin.org/article/10.3389/fphy.2021.639389`.

[59] Katrin H Preller et al. "Changes in global and thalamic brain connectivity in LSD-induced altered states of consciousness are attributable to the 5-HT2A receptor". en. In: *Elife* 7 (Oct. 2018).

[60] Katrin H Preller et al. "Effective connectivity changes in LSD-induced altered states of consciousness in humans". en. In: *Proc. Natl. Acad. Sci. U. S. A.* 116.7 (Feb. 2019), pp. 2743–2748.

[61] Gunnar Pruessner. *Self-Organised Criticality*. Cambridge, England: Cambridge University Press, Aug. 2012.

[62] Dante R. Chialvo. "Critical brain networks". en. In: *Physica A* 340.4 (Sept. 2004), pp. 756–765.

[63] G Ruffini and G Deco. "The 2D Ising model, criticality and AIT". Oct. 2021.

[64] G. Ruffini. "An algorithmic information theory of consciousness". In: *Neurosci Conscious* (2017). DOI: `10.1093/nc/nix019.PMID:30042851`.

[65] Giulio Ruffini. "Application of the reciprocity theorem to EEG inversion and optimization of EEG-driven transcranial current stimulation (tCS, including tDCS, tACS, tRNS)". In: *arXiv:1506.04835* (2015).

[66] Giulio Ruffini. "Lempel-Ziv Complexity Reference". In: *arXiv:1707.09848 [cs.IT]* (2017).

[67] Giulio Ruffini and Edmundo Lopez-Sola. *AIT foundations of structured experience*. June 2022. DOI: 10.31234/osf.io/k3q6r. URL: psyarxiv.com/k3q6r.

[68] Giulio Ruffini et al. "EEG-driven RNN classification for prognosis of neurodegeneration in at-risk patients". In: *ICANN 2016* (2016).

[69] Giulio Ruffini et al. "Targeting brain networks with multichannel transcranial current stimulation (tCS)". In: *Current Opinion in Biomedical Engineering* (2018).

[70] Michael M. Schartner et al. "Increased spontaneous MEG signal diversity for psychoactive doses of ketamine, LSD and psilocybin". In: *Scientific Reports* 7.46421 (2017).

[71] Elad Schneidman et al. "Weak pairwise correlations imply strongly correlated network states in a neural population". In: *Nature* 440.20 (2006), pp. 1007–10112.

[72] Woodrow L Shew and Dietmar Plenz. "The functional benefits of criticality in the cortex". en. In: *Neuroscientist* 19.1 (Feb. 2013), pp. 88–100.

[73] S Parker Singleton et al. "LSD and psilocybin flatten the brain's energy landscape: insights from receptor-informed network control theory". May 2021.

[74] Enzo Tagliazucchi et al. "Criticality in large-scale brain FMRI dynamics unveiled by a novel point process analysis". In: *Front. Physiol.* 3 (Feb. 2012), p. 15.

[75] Enzo Tagliazucchi et al. "Increased global functional connectivity correlates with LSD-induced ego dissolution". en. In: *Curr. Biol.* 26.8 (Apr. 2016), pp. 1043–1050.

[76] Daniel Toker et al. "Consciousness is supported by near-critical slow cortical electrodynamics". en. In: *Proc. Natl. Acad. Sci. U. S. A.* 119.7 (Feb. 2022), e2024455119.

[77] N. Tzourio-Mazoyer et al. "Automated anatomical labeling of activations in SPM using a macroscopic anatomical parcellation of the MNI MRI single-subject brain". In: *NeuroImage* 15.1 (2002), pp. 273–289. ISSN: 10538119. DOI: 10.1006/nimg.2001.0978.

[78] Thomas F Varley et al. "Serotonergic psychedelics LSD & psilocybin increase the fractal dimension of cortical brain activity in spatial and temporal domains". en. In: *Neuroimage* 220.117049 (Oct. 2020), p. 117049.

[79] Terry Welch. "A Technique for High-Performance Data Compression". In: *Computer* 17.6 (1984), pp. 8–18.

[80] Shan Yu et al. "Universal organization of resting brain activity at the thermodynamic critical point". en. In: *Front. Syst. Neurosci.* 7 (Aug. 2013), p. 42.

[81] Hector Zenil et al. "A Decomposition Method for Global Evaluation of Shannon Entropy and Local Estimations of Algorithmic Complexity". In: *Entropy* 20.8 (2018). ISSN: 1099-4300. DOI: 10.3390/e20080605. URL: https://www.mdpi.com/1099-4300/20/8/605.

[82] Xu-Sheng Zhang, Rob J. Roy, and Erik Weber Jensen. "EEG Complexity as a Measure of Depth of Anesthesia for Patients". In: *IEEE Transactions on Biomedical Engineering* 48.12 (2001), pp. 1424–1433.

[83] Vincent Zimmern. "Why brain criticality is clinically relevant: A scoping review". en. In: *Front. Neural Circuits* 14 (Aug. 2020), p. 54.